Title
Cavitation-Induced Stiffness Reductions in Quantum Dot–Polymer Nanocomposites

Journal
Chemistry of Materials, 28(8)

ISSN
0897-4756

Authors
Raja, Shilpa N
Luong, Andrew J
Zhang, Wencong
et al.

Publication Date
2016-04-26

DOI
10.1021/acs.chemmater.5b04165

Peer reviewed

CHEMISTRY OF MATERIALS

Article

pubs.acs.org/cm

Cavitation-Induced Stiffness Reductions in Quantum Dot−Polymer Nanocomposites

Shilpa N. Raja,[†,‡] Andrew J. Luong,[§] Wencong Zhang,[§] Liwei Lin,[∥] Robert O. Ritchie,[*,†,‡,∥] and A. Paul Alivisatos[*,†,‡,⊥,#]

[†]Materials Sciences Division, Lawrence Berkeley National Laboratory, Berkeley, California 94720, United States

[‡]Department of Materials Science and Engineering, [§]Department of Chemical Engineering, [∥]Department of Mechanical Engineering, and [⊥]Department of Chemistry, University of California, Berkeley, California 94720, United States

[#]Kavli Energy NanoScience Institute, Berkeley, California 94720, United States

Supporting Information

ABSTRACT: The elastic stiffness of two polymer nanocomposite systems is investigated. The nanoscale fillers comprise cadmium selenide (CdSe, ∼4 nm) and cadmium selenide/cadmium sulfide (CdSe/CdS, ∼13 nm) quantum dots (QDs). The QDs are embedded within an electrospun structural block copolymer, poly(styrene-ethylene-butylene-styrene) (SEBS). Tensile testing shows a monotonic decrease in the tensile Young's modulus with increasing partially phase-separated QD concentration; this is to be compared to corresponding nanocomposites reinforced with nanorod (NR) and tetrapod (TP)-SEBS nanocomposites which show a monotonic increase with particle loading. While most studies to date emphasize the increase in Young's modulus in polymer nanocomposites at higher reinforcement loadings, few focus on the tunability of the modulus from *reductions* in stiffness. The present work reveals up to an ∼80% reduction in tensile Young's modulus with the addition of 5 vol % of QDs to electrospun SEBS. In this study, we sought mechanistic insight into this reduction in composite stiffness using a 2D lattice spring model. Simulation results reveal that the stiffness decrease with the addition of QD reinforcements is likely due to cavitation in the polymer in the vicinity of the QD aggregates arising from polymer debonding under tension. We anticipate that this study, performed with a commonly used structural rubber, may find use in designing polymer−matrix nanocomposite fibers with specific Young's moduli for applications requiring a tunable lower stiffness material.

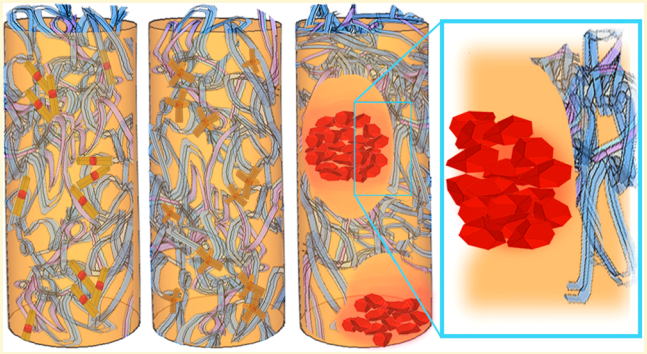

INTRODUCTION

Polymeric nanocomposites show considerable promise as structural materials due to their high filler−polymer surface area,[1−11] including mechanical improvements at very low reinforcement loadings,[1,3,5,7−14] stiffness enhancements due to nanoscale branching,[12−16] and synergistic nanocarbon reinforcement effects,[2,4,6,7,17] to name but a few.[1,3,5,7−11,18] The desirable mechanical properties of these nanocomposites depend in large measure upon the chemistry of the interface between two components with significantly different moduli.

Most studies on nanocomposite fillers reveal a progressive increase in modulus with increasing reinforcement volume fractions; examples of studies in polymers include clay-based nanocomposites,[12−14,19,20] microscale ceramic TPs and needles,[15,16,21] graphene,[17,22] carbon nanotubes,[13,18,23−27] carbon black,[3,8,10,19,20,22,28−31] glass fibers,[3,8,10,21,32−34] and others.[22,35−37] This clearly is to be expected from a rule of mixtures analysis[4,7,13,23−27] owing to the much higher Young's modulus of the filler.[1,3,5,8,10,22,28−31] Fewer studies have shown the opposite effect, that of a reduction in Young's modulus.[3,8,10,12,14,32−34] For example, it has been reported for bioinspired nanocellulose−rubber composite materials where the Young's modulus decreased by 40 times through exposure to small chemical moieties that regulated nanofiller−polymer interaction,[2,6,35−37] in silicon cantilevers in which the Young's modulus decreased monotonically by three times with cantilever thickness,[4,7] and in pure polymers and metallic thin films where a two to five times stiffness decrease was seen due to humidity[1,5] and temperature;[12] additionally a thirty-fold decrease in hardness has been reported by introducing acid or small oligomers into a polymer matrix to disrupt interchain bonds.[2,6] Here we examine a case where there is a significant modulus reduction in a nanofiller−polymer nanocomposite in which the nanofiller is of 1000 to 2000 times higher stiffness than the polymer matrix. Previous studies on polymer nanocomposites have revealed reductions of 1−15% based on

Received: October 27, 2015
Revised: March 25, 2016
Published: March 27, 2016

DOI: 10.1021/acs.chemmater.5b04165
Chem. Mater. 2016, 28, 2540−2549

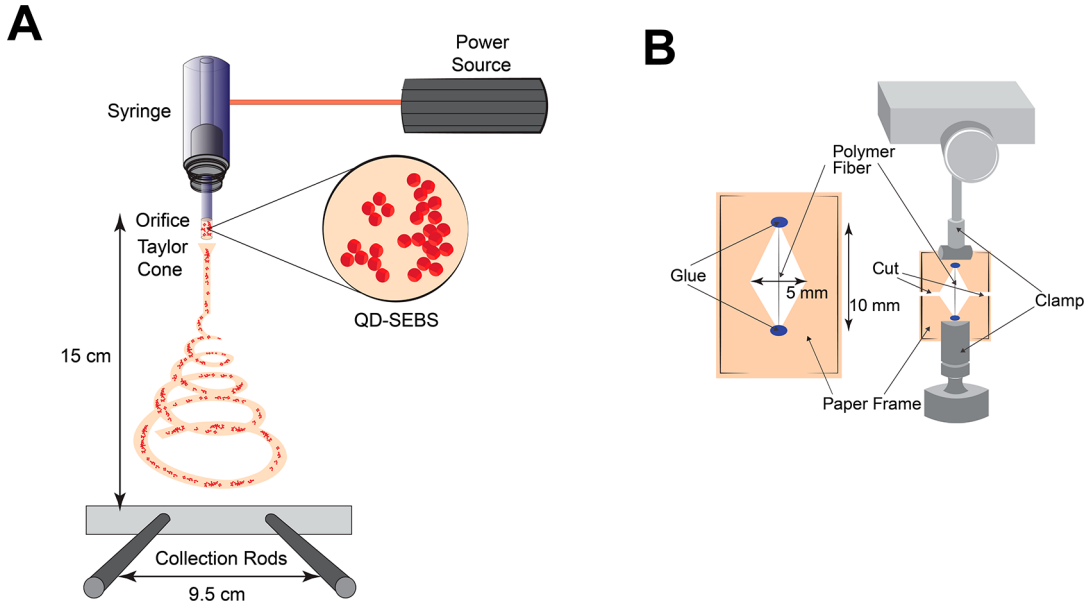

Figure 1. Schematic of electrospinning and uniaxial tensile testing. (A) Schematic of electrospinning process of QD−SEBS nanocomposite fibers. (B) Schematic of cardboard tab with electrospun fiber glued across diamond opening and mounting into tensile tester using clamps. Black double arrow indicates stretching direction.

tensile testing of nanocomposites with volume percents of 0.1−5% (including where the nanoparticles were partially phase-separated).[3,7−11,38] Higher reductions have been predicted for higher filler fractions, but they have not previously been experimentally realized. Achieving higher reductions in the tensile Young's modulus could provide a larger design space for these materials, thereby facilitating the design of nanocomposites with elastic stiffnesses better optimized for specific applications.[28]

It is possible for voids to open up at the polymer−filler interface under tension, and the resulting cavitation can dramatically influence the Young's modulus of the nanocomposites. Here we investigate this effect in nanocomposites with partially phase-separated cadmium selenide (CdSe) and cadmium selenide/cadmium sulfide (CdSe/CdS) QD fillers in the widely used block copolymer poly(styrene-ethylene-butylene-styrene) (SEBS). Although both fillers have 3 orders of magnitude higher stiffness than the host polymer,[13,23−27] we find that the resulting QD−SEBS nanocomposites, with phase-separated QDs, display an ∼45−80% lower tensile Young's modulus than the unreinforced matrix. While the mechanical properties of nanoscale fillers in electrospun polymers have been widely studied,[14,16,39−44] this study is the first to report a Young's modulus reduction and represents the largest such effect reported in the literature to date in any polymer−nanoparticle composite.[3,8,10,22,28−31]

Previous results have shown smaller but similar (∼1−15%) stiffness reductions within the range of 0.1−5 vol % filler contents, which were attributed to weak interfaces or cavitation of the filler particles.[3,8,10,22,28−31] We examine our results here through a comparison with a nanoparticle−polymer lattice spring model (LSM) which provides mechanistic insights into this effect. This model suggests that the reduction in Young's modulus for the QD−SEBS nanocomposites is due to the formation of cavities in the vicinity of the QD assemblies in the polymer matrix. The cavities form because of the nature of the chemical bonding at that interface, which is comparatively weak due to the nanoparticle surface chemistry and the processing conditions used in this study.[45] Direct visualization of such cavities around nanoparticles in structural composites via optical or transmission electron microscopy remains challenging,[3,8,10,32−34] especially in the early stages of void formation. The LSM simulation provides a facile way to qualitatively model this effect, albeit in two dimensions, in partially phase-separated nanocomposites where the Young's modulus is lowered when a higher stiffness filler is added. In this particular case, we seek to find a means to tailor the chemical nature of the interface between the polymer and nanoparticle using processing techniques that can result in the tunability of a key material property, i.e., the Young's modulus.

RESULTS AND DISCUSSION

Electrospinning, Fiber Collection, and Tensile Testing.

CdSe QDs ∼4 nm in diameter, large CdSe/CdS core/shell QDs (LQDs) ∼13 nm in diameter, and NRs and TPs of ∼25 nm arm length were prepared via established protocols (see Materials and Methods section for further details).[46,47] The QDs were incorporated into poly(styrene-ethylene-butylene-styrene) (SEBS) polymer matrices via electrospinning.[9,14] A schematic of the electrospinning process is shown in Figure 1A. The lamellar SEBS (Kraton, MD1537) had a molecular weight of 117 000 Da and consisted of 60% polystyrene.[14] Electrospinning was performed from solutions of SEBS polymer in chloroform at concentrations of 12% SEBS by weight of chloroform and appropriate amounts of QDs to achieve concentrations of 5, 10, and 20% by weight for each shape.[14] Briefly, a 1 kV/cm electric field was applied to a droplet of polymer solution at the end of a #21 gauge needle of ∼500 um diameter.[14] The fiber collector geometry of Li et al., consisting of a double rod collector spaced 80 mm apart, was used to obtain an array of single fibers that could be collected individually.[48] After fiber collection, single fibers were glued with epoxy to cardboard tabs with diamond cutouts and mounted between parallel grips in an Agilent T-150 tensile testing machine (Figure 1B). Samples were mechanically tested using a quasi-static strain rate of 6.9×10^{-3}.

DOI: 10.1021/acs.chemmater.5b04165
Chem. Mater. 2016, 28, 2540−2549

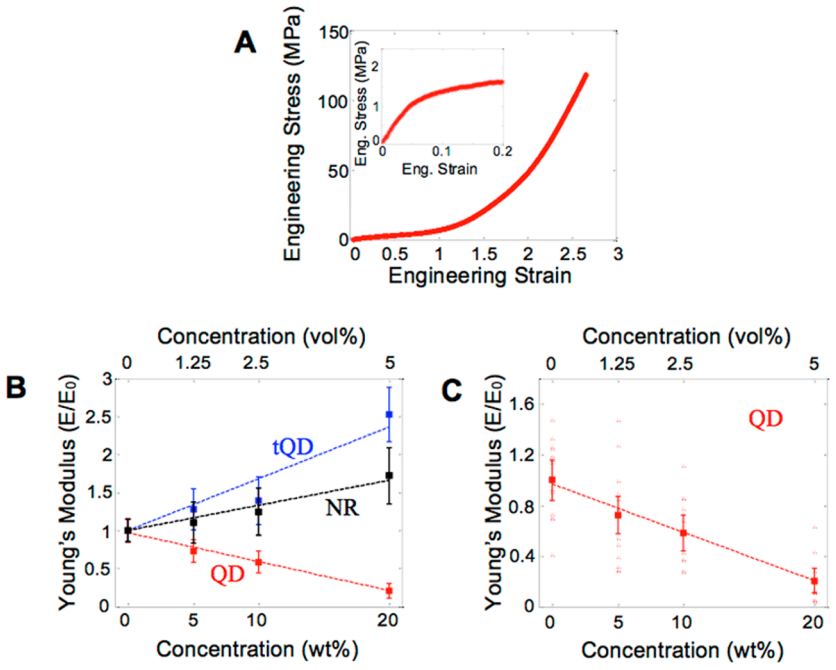

Figure 2. Uniaxial tensile stress−strain curves of TP and NR−SEBS polymer nanocomposites. (A) Typical stress−strain curve of 5 wt % QD nanocomposites, with inset highlighting the elastic region occurring from ∼0−5% strain. (B) Plot of normalized Young's modulus as a function of concentration for TP, NR, and QD−SEBS nanocomposites. (C) Young's modulus as a function of concentration for QD−SEBS nanocomposites. Each red "x" represents a data point from a single tensile test.

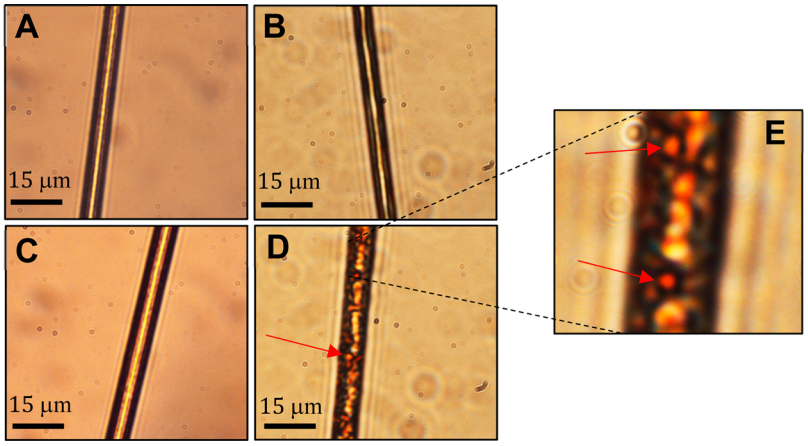

Figure 3. Optical micrographs of the electrospun fibers. (A) Fibers with no QDs. (B) Fiber with 10% NR. (C) Fiber with 10% TP. (D) Fiber with 10% QD. (E) Inset of fiber shown in subfigure F. Red arrows indicate optically visible red QD aggregates.

Figure 2A illustrates a typical uniaxial mechanical stress−strain curve to failure for the 5% QDs nanocomposites; further examples of such uniaxial stress−strain curves can be seen in SI Figure 1 of the Supporting Information. The slope of the linear region of the curves in the small-displacement elastic limit (at less than 0.03 strain) was used to determine the Young's modulus. Additional information on these procedures is described elsewhere.[14] Figure 2B illustrates the normalized Young's modulus for TP, NR ,and QD−SEBS nanocomposites as a function of concentration. These data show that the addition of TPs and NRs in, respectively, TP−SEBS and NR−SEBS nanocomposites displays the expected enhancements in Young's modulus with increasing filler concentration,[8,14,28] as predicted by law of mixtures analysis that gives stiffness increases in composites consisting of a very stiff filler embedded in a relatively weak matrix material. The partially phase-separated QD−SEBS nanocomposites conversely exhibit exactly the opposite behavior with a monotonic decrease in stiffness with increasing QD concentration.[3,8,10,28]

The magnitude of the observed reduction in tensile Young's modulus is especially large—up to 5 times at 20% filler addition by weight (5% addition by volume). Previous theoretical and experimental studies, including analytical work on the rule of mixture theories that account for the formation of small cavities in the particle vicinity, have shown decreases in the range of 1−15% for nanoparticle−polymer composites.[3,8,10] Figure 2C illustrates the QD−SEBS elastic modulus curve as a function of concentration (third curve in Figure 2B) with raw data points overlaid. A total of 10−15 samples were tested for each data point. As can be seen, there is a high degree of scatter in the raw data, which has been previously observed and is likely attributable to the large amount of variation in electrospun fiber

DOI: 10.1021/acs.chemmater.5b04165
Chem. Mater. 2016, 28, 2540−2549

microstructures due to varying electric fields and fast fiber drying times during electrospinning.[42,45]

Figure 3 illustrates optical micrographs of fibers with no QDs (Figure 3A) as well as NR (Figure 3B), TP (Figure 3C), and QD−SEBS (Figure 3D) fibers. Fibers, ranging from 1.5 to 6 μm in diameter, showed no dependence of Young's modulus on the fiber diameter. As seen in the images, the fiber morphology was relatively uniform for those with no nanoparticles as well those with TPs and NRs. However, red circular assemblies, ∼1−3 μm in size, could be seen in optical images in the vicinity of the QD fibers at all concentrations (Figure 3E). On the basis of TEM characterization (Figure 4), these red areas most likely represent large visible aggregates of QDs. In light of these observations, it is likely that the marked decrease in Young's modulus with increasing QD concentrations is associated with the phenomena of cavitation, where voids form in the polymer during tensile drawing; the extent of such cavitation is known to scale with the size of different types of matrix inclusions (such as glass, rubber, and others) and to not occur below a critical inclusion size.[30,31] This may explain why such apparent cavitation was seen in QD nanocomposites but not for the TP and NR nanocomposites, which have much smaller nanoparticle assemblies (SI Figure 2).[14]

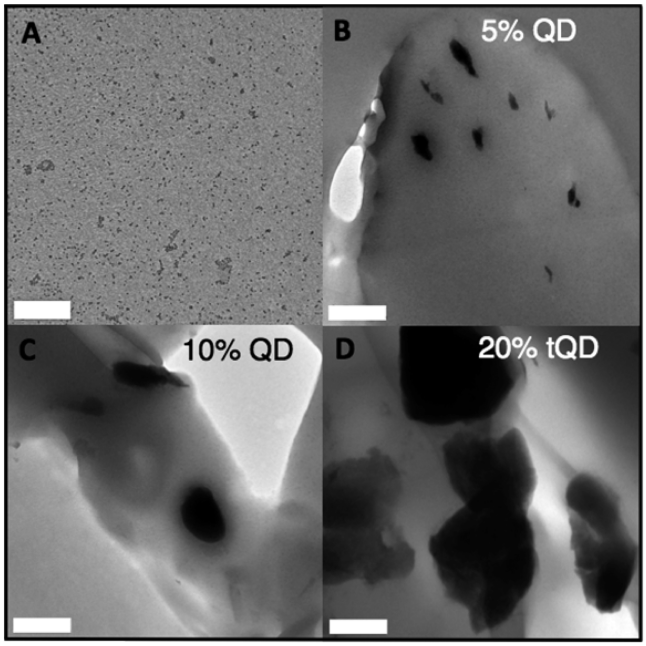

Figure 4. Transmission electron micrographs of QDs and QD−Polymer Nanocomposites. TEM micrographs of (A) QDs before polymer integration, (B) 5 wt % QD−polymer nanocomposites, (C) 10 wt % QD−polymer nanocomposites, and (D) 20 wt % QD−polymer nanocomposites. Scale bar in A is 200 nm, and scale bars in B−D are 500 nm.

Decreases in Young's modulus of polymer nanocomposites, albeit smaller than the ones in this work, have been observed before by other mechanisms. Neitzel et al. observed ∼15% decreases in Young's modulus by including amine-passivated nanodiamonds into epoxy but attributed this to the amine groups on the nanodiamonds interfering with the curing of the epoxy.[38] As the processing technique used to prepare the nanocomposites in our work does not involve curing, this is unlikely to be the mechanism for our observed decrease. Nonmonotonic behavior in the Young's modulus with increasing fill fraction has also been observed when the polymer and filler phase have very different coefficients of thermal expansion and thus develop internal stresses during cooling from high-temperature curing or molding; this is unlikely the mechanism in this work since our processing occurs at room temperature.[49]

Electrospinning is a tensile drawing process known to result in voids formed via cavitation due to fast drying times and very high tensile drawing forces during the fiber formation under high electric fields.[45] Even if voids do not fully form, the cavitation process involves the stretching out and thinning of chains in high mobility regions, possibly resulting in a weak interface between the QD aggregate and the polymer, which in turn could readily debond to form a cavity at the QD−polymer interface upon stretching in the small-displacement elastic regime.[3,33,50] Previous work in the literature on similar CdSe and CdS QD−polymer nanocomposite systems with identical QD surface chemistry involves nanocomposites which were processed via film casting. In these studies, only increases in the Young's modulus at all concentrations were observed at all concentrations,[22,51−53] indicating that the processing technique in this work is critical for the stiffness reductions observed.

As noted above, only rule of mixtures theories which accounted for cavitation[3,8] predict decreases in the Young's modulus of polymer composites, albeit smaller than those observed in this work. Several experimental and theoretical studies have concluded that larger particles or aggregates in polymers form larger associated cavities,[30,31,54,55] with no cavitation below a critical inclusion cutoff size. Previous work has shown that TPs and NRs at the same concentrations in SEBS can increase the Young's modulus.[14] This is not due to a difference in surface chemistry, because TPs, NRs, and QDs are all coated with alkyl-chain ligands;[46,47] on the contrary, this is likely because TP and NR aggregates are on average much smaller than the QD aggregates (SI Figure 2) and are below the critical size for cavitation.[30,31,54,55]

Dispersion of the QDs in the SEBS Polymer. The much larger aggregates for the QD−SEBS nanocomposites, as compared to the TP and NR−SEBS systems, can also be seen in our TEM micrographs in Figure 4. (The 4 nm CdSe QD composites are shown in the main text; the nanoparticle dispersion in the LQD−SEBS composites is shown in SI Figure 3). Likely due to the relative chemical dissimilarity of the native alkyl chain ligands on the QDs and the 60% polystyrene phase, the nanoparticles in all systems form aggregates distributed throughout the SEBS polymer.[56] Figure 4 shows TEM micrographs of QDs (a) before and (b−d) after integration into the polymer matrix. The QD aggregates in the 10% and 20% nanocomposites are ∼1 order of magnitude larger than the aggregates seen in the 5% nanocomposites (SI Figure 2). They are also approximately 1 order of magnitude larger than the aggregates in the TP and NR nanocomposites.

Since such exceptionally large aggregates only exist in the QD systems with the decreased moduli and not in any of the TP and NR nanocomposites, these large aggregates in the 10 and 20 wt % QD nanocomposites (Figure 4C,D, SI Figure 2) may serve as nucleation sites for cavities in the polymer matrix during electrospinning.

Cavities formed during tensile drawing processes of polystyrene or its block copolymers tend to nucleate early in the elastic regime.[3,50,57] While the aggregates in the 5% QD−SEBS nanocomposites are on average the same size as the TP and NR composites, the standard deviation is much greater,

DOI: 10.1021/acs.chemmater.5b04165
Chem. Mater. 2016, 28, 2540−2549

meaning that there are some aggregates that are far larger, i.e., comparable to the average size of 10% and 20% QD−SEBS composites (SI Figures 2, 4). This may explain the observed Young's modulus decrease for the 5% QD−SEBS composites.

The cavities are not readily visible in TEM images because of the minimal electron diffraction contrast between polymers and cavities, especially since the latter do not extend through the entire microtomed cross-sectioned sample. The very high contrast of the QD aggregate reduces the ability to differentiate between the cavities and the polymer. Attempts to improve contrast using longer dwell times and narrower objective apertures did not improve resolution of the cavities. It is further possible that the effect is due to cavities which form in the early elastic region during the tensile mechanical testing of our polymers rather than during electrospinning, since the electrospinning process around larger aggregates may result in a much weaker, lower-density interface which may immediately debond upon the initiation of tensile drawing.[3,50,58] Indeed, optically visible voids or crazes (>∼200 nm) have been observed in the early elastic region (∼1.5% strain, before the yield point) in SEBS polymer.[50] This indicates that voids, too small to be optically resolved, can be readily nucleated due to the brittle nature of polystyrene.[50]

This is in line with with previous analytical theories of the mechanical properties of cavitated composites.[3,59] In these studies, the underlying assumption was that cavities were present immediately after the start of tensile testing but not before. Cavities nucleate after the start of tensile testing due to the weak nature of the chemical interface between the inclusion and polymer.[3,59] Further support for this assumption of postprocessing cavity nucleation in our particular case is that the polymer in our study, SEBS, is a thermoplastic elastomer which behaves like a lightly cross-linked natural rubber.[28] We have observed that even after stretching to over 100% percent strain, the polymer rebounds fully to its original dimensions nearly immediately, as expected for lightly cross-linked rubbers. Furthermore, the polymers exhibit a similar Young's modulus even after several cycles of loading and unloading.[28] This indicates that even if cavities form during electrospinning, they may disappear as the polymer rebounds, since there is an interval of hours between electrospinning and mechanical testing. The cavities may then form again in the early stages of tensile drawing due to the weak interface, which leads to debonding.[58]

Compression or shear tests can be used to provide evidence of cavitation and to determine if cavitation is occurring before or after a tensile test.[28] However, while all studies show decreases in the tensile bulk modulus from cavitation,[60] the comprehensive article of Dorfmann et al. shows there is no effect of cavitation on the compressive bulk modulus or shear modulus of cavitated structural rubbers.[60] Additionally, compression tests have not yet been successfully performed on single electrospun fibers, which typically have a diameter of 0.2−10 μm (1−5 μm in this work).[61] Shear tests are very challenging to perform on single electrospun fibers, and shear moduli of such thin fibers must be indirectly inferred from AFM bending tests using specialized and custom-built testing techniques.[28,40]

We performed several simulations to explore cavitation as a possible explanation for the experimentally observed modulus decrease.

LSM Simulations of the QD Nanocomposites with Cavitation. QD nanocomposites were simulated using a 2D nanoparticle−polymer LSM (Figure 5).[62] LSMs are an alternative to finite element models[63] and have been used extensively to simulate the mechanical properties of polymer nanocomposites.[43,44,62,64−67] Several assumptions were used in the simulations. Specifically, a known Young's modulus difference was incorporated between the QD and polymer.[14,32,33] In addition, based on previous experimental observations,[3,32−34] the cavities were assumed to be elliptical, aligned with the tensile axis, and to span the entire size of the aggregate. Further details are given below (see Materials and Methods).

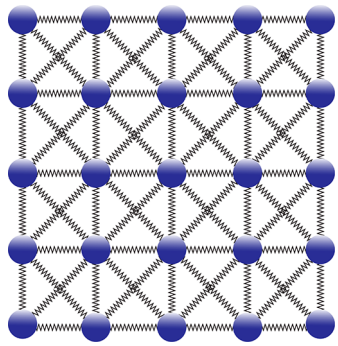

Figure 5. Schematic of 2D simple square data structure utilized in the LSM. The LSM consists of nodes (spheres in the diagram) with hookean springs joining nearest and next-nearest neighbors.

Using this approach,[14,28] the LSM simulations were found to be in good agreement with experiment with the inclusion of voids in the vicinity of the nanoparticle−polymer interfaces. Based on these simulations, the large reductions in elastic modulus are likely explained by cavitation for both ∼4 nm CdSe QD−SEBS and ∼13 nm CdSe/CdS LQD−SEBS partially phase-separated nanocomposites. Figure 6 illustrates the elastic strain fields after stretching of the 5, 10, and 20% ∼4 nm CdSe QD−SEBS simulated nanocomposites (corresponding strain fields and experimental-theoretical comparisons for the LQD−SEBS nancomposites are shown in SI Figures 5 and 6). As can be seen in Figure 3, the cavities undergo an expected extensional elongation parallel to the uniaxial tensile direction, with strain concentrated at the cavity edges as the cavity acts as a defect; red regions correspond to the highest strains and dark blue regions to lower strains. Restriction of the polymer matrix at the transverse edges of the nanoparticle aggregate results in a high concentration adjacent to it, resulting in the observed regions of high strain in Figure 3.

Figure 7 gives a graphical comparison of the experimental and simulated Young's moduli. The experimentally observed reductions in the Young's modulus ranged from 27 to 78% for the 5 to 20 wt % concentrations for the QD−SEBS nanocomposites and from 40 to 65% for the 5 to 20 wt % concentrations for the LQD−SEBS nanocomposites (Figure 7 and SI Figure 6). The LSM simulations matched this decrease in Young's modulus with increasing reinforcement concentration for both nanocomposites when cavities were included in the model. Qualitatively, reasonable agreement was found for the values for the elastic moduli and the trendline of best fit of the elastic modulus as a function of concentration, highlighted in Figure 4 and SI Table 1. (See SI Figure 6 for comparable data on the LQD−SEBS nanocomposites and subheading S1 in the Supporting Information for a discussion of the differences in the stiffness reductions for the two nanocomposite systems).

DOI: 10.1021/acs.chemmater.5b04165
Chem. Mater. 2016, 28, 2540−2549

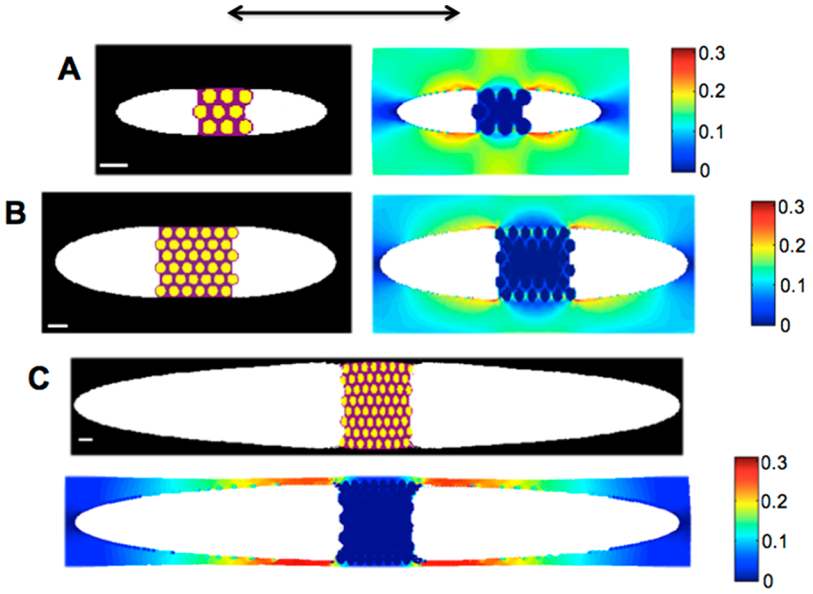

Figure 6. Simulations of QD−SEBS nanocomposites using a lattice-spring model (LSM). (A) (Left) LSM spring distribution image before stretching for 5 wt % hexagonal close-packed (HCP) QD−SEBS nanocomposites; yellow represents QD, purple represents interface, and black represents polymer. (Right) Elastic strain field after stretching. Black double arrows indicate the stretching direction. (B) Corresponding images for the 10 wt % HCP-packed QD−SEBS nanocomposites. (C) Corresponding images for the 20 wt % HCP-packed QD−SEBS nanocomposites. Scale bars are 4 nm for all images.

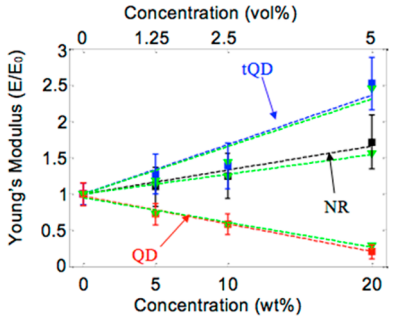

Figure 7. Comparison of experimental results with simulated results from lattice-spring model. Comparison of theoretical−experimental agreement for TPs, NRs, and QDs (dashed lines and green markers represent simulated results, without cavitation for TPs and NRs and with cavitation for QDs).

For the 5 and 10% QD concentrations by weight, the cavity size in the simulation increases linearly (as does the aggregate size, shown from an analysis of our transmission electron microscopy TEM images in SI Figure 2). On the other hand, cavities in the 20% QD concentration composites are two times greater than the expected value from a linear increase. For 5 and 10% CdSe QD−SEBS nanocomposites, the ratio of the major axis of the elliptical cavities to the aggregate diameter is 1.3 and 1.5, respectively, while for the 20% nanocomposite, the cavities are 4.1 times the aggregate diameter. This greater size increase for the cavities in the 20% by weight nanocomposite is possibly due to intercavity coupling; at higher concentrations, large aggregates are closer together, which causes their cavities to interact. Thus, each QD aggregate experiences a larger effective cavity size. (A further discussion of how cavity sizes change with concentration in the LQD−SEBS nanocomposites is given in the Supporting Information).

Additionally, the intercavity coupling may be enhanced at the highest concentrations because of electrospun fiber structure. Electrospun fibers tend to have more cavities in the outer sheath because of their high surface area which leads to a fast drying time;[14,45] this may indicate that large aggregates nearer the surface have more cavities in their vicinity. Due to the high frequency of aggregates in the 20% QD−polymer nanocomposites as compared to the 5% QD−polymer nanocomposites, there is a higher probability that an aggregate will appear at the fiber surface at the highest concentrations. In the 20% QD−polymer nanocomposites there are thus likely more massive aggregates at the fiber surface. Though the 5% composites also have very large aggregates (SI Figure 4), they are less likely to be found at the surface of the fiber due to their lower density.

We have simulated the Young's modulus of different QDs and polymers with modulus value ranges of 10−4000 times that of the polymer and found that the modulus ratio within this range, as well as the modulus of the polymer matrix, creates minimal difference in the stiffness reduction profile. This stiffness range encompasses the vast majority of metallic and ceramic materials as well as very soft and hard polymers.[28] Thus, from our simulations, it is apparent that this stiffness reduction phenomenon will happen for polymer nanocomposites consisting of other ceramic and metallic nanoparticles and diverse polymer systems.

One explanation for this is that the cavities effectively isolate the nanoparticles from the polymer matrix. This means that nanoparticle−polymer interfacial chemistry (which affects interface strength, debonding of the polymer−QD interface, and the cavity size) is of greater importance than the modulus of the filler.[3,10,37,48]

Figure 8 shows the effect of changing cavity size and shape on the simulated stiffness for the 10 wt % QD−SEBS nanocomposite. The black line shows the experimental result; arrows indicate the different simulated cases. Only elliptical-shaped cavities aligned parallel to the stretching axis (to the left and right of the images in Figure 8) gave good agreement with

DOI: 10.1021/acs.chemmater.5b04165
Chem. Mater. 2016, 28, 2540−2549

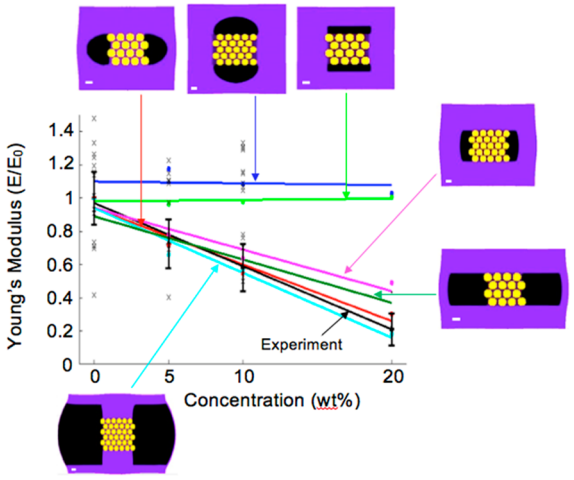

Figure 8. Effect of changing cavity size and shape on simulated stiffness of QD−polymer nanocomposites. Plot showing the effect of changing cavity size and shape on the Young's modulus. Lines of best fit to data points for each type of simulated cavity are shown. Pictures indicate the simulated cavity size and shape. Scale bars are 4 nm.

experiment (red and black lines in Figure 8). Other conditions, such as rectangular cavities, cavities perpendicular to the stretching axis (blue and light green arrows), or cavities that spanned past the aggregate (teal arrow), gave relatively poor agreement with experiment, as evidenced by the best fit lines and data points in Figure 8. These results are consistent with previous theoretical predictions and experimental results using X-ray diffraction and thermal imaging, in that cavities, aligned with an elliptical stretching axis and that spanned the aggregate body, gave the best agreement with the experimental findings. Furthermore, changing the aggregate packing from HCP to loose-packed structures was found to minimally affect the agreement between experiment and theory as compared to cavity size, shape, and orientation (SI Figure 7), an observation that we believe results from the cavities essentially isolating the aggregates from the polymer matrix.

As noted, previous studies have found reductions of 1−15% in the tensile Young's modulus through reinforcement of a polymer matrix with high stiffness nanoparticles or other inclusions.[3,8,10,14] Here we have found that additions of 5 vol % of phase-separated QDs that are over 3 orders of magnitude stiffer than a host polymer can decrease the Young's modulus by as much as 80%; indeed, we have seen this phenomenon in two block copolymer nanocomposites with two different QD−nanoparticle systems. In contrast, our identically prepared SEBS nanocomposites reinforced with 5 vol % of TPs or NRs displayed increases of 70−150% in modulus.

Nanoscale fillers in electrospun polymers have been extensively studied in a variety of ways, including the mechanical properties of single electrospun fibers and electrospun mats.[14,16,39−44,63] However, compared to all of these studies, the current investigation is the only one to report a reduction in the Young's modulus with increasing filler content. Our work is also the only study of any polymer−nanoparticle composite to achieve such high degrees of reduction. The insights provided by LSM simulations may prove of relevance to structural designs and to the tunability of Young's modulus in structural composites, in particular because cavitation, the process that we attribute these observations to, is known to occur in common structural processing techniques for polymer fibers.[28,32,33]

CONCLUSIONS

In summary, we have studied the elastic modulus of structural QD−SEBS polymer nanocomposites experimentally and by simulation. We have seen a very significant reduction of 43−80% in the tensile Young's modulus for polymer nanocomposites reinforced with phase-separated QDs that are over 1000 times stiffer than the polymer matrix. Using two-dimensional lattice spring model simulations, we attribute this decrease to cavitation in the vicinity of the nanoparticle−polymer interfaces, created during tensile drawing. To achieve good agreement between the experimentally obtained and simulated Young's moduli for the two systems, it was necessary to assume the presence of elliptical cavities oriented parallel to the stretching direction, consistent with previous theoretical predictions and diffraction and thermal studies.[32−34] By accounting for experimental parameters such as interface strength, cavitation, filler orientation and shape, and aggregation and matrix structure, good matching between simulation and experiment was achieved. We conclude that lattice spring model simulations provide a useful tool for engineering the properties of polymer−matrix nanocomposites that have undergone cavitation during processing. Direct cavity visualization around matrix inclusions in the early elastic region is a significant challenge and usually must be inferred indirectly. Our simulation technique can provide a basic tool to qualitatively account for the presence and impacts of such cavities. The approach followed in this work may help to shed light on how to engineer the elastic moduli of structural polymeric nanocomposite fibers within an expanded range of downward tunabilities using cavitation.

MATERIALS AND METHODS

Since many of the experimental and simulation methods used here were identical to those described previously,[14] they are only briefly described below with small changes noted.

Materials. All chemicals used were purchased from Sigma-Aldrich. SEBS polymer was kindly provided by Kraton corporation (MD1537, white powder).

Synthesis of CdSe QDs. CdSe QDs of diameter 4.0 ± 0.5 nm and core/shell CdSe/CdS QDs of diameter 13.0 ± 1.0 nm were synthesized and cleaned, as reported previously.[46,47]

Preparation of QD−Polymer Precursor Solutions for Electrospinning and Film Casting. Chloroform solutions containing appropriate concentrations of native CdSe QDs (no ligand exchange performed) were mixed with premixed polymer−chloroform solutions to create solutions of 12% SEBS by weight in chloroform with 5%, 10%, and 20% nanoparticle incorporation by weight of polymer. Solutions were typically made with 25 mg SEBS polymer and about 0.5 mL of chloroform in order to achieve the high viscosity needed for electrospinning. Due to the excellent solubility of the polymer in chloroform, dissolution was observed to occur within minutes. Regardless, solutions were vortexed for several hours to ensure uniformity.

Electrospinning of TP−SEBS Composite Single Fibers. Electrospinning was performed using a bias of 15 kV between the collector and syringe needle and collector-syringe needle distance of 150 mm for all runs (electric field of 1 kV/cm). For all samples, needles purchased from Nordson Corporation (part number 7018225, #21 gauge, 38.1 mm gauge length, 0.51 mm inner diameter) were used. Approximately 0.1−0.2 mL of solution was loaded into the syringe, and a droplet of solution was manually ejected immediately prior to turning on the power supplies. Chloroform (Sigma-Aldrich) was used as the electrospinning solvent.

DOI: 10.1021/acs.chemmater.5b04165
Chem. Mater. 2016, 28, 2540−2549

Single fibers of diameter 2−6 μm were fabricated using the collector design of Li et al.,[48] consisting of two metal rods of 8 mm diameter spaced 95 mm apart. Electrospinning was conducted in a fume hood set to low flow to avoid damage of fibers. Care was taken to ensure identical conditions of voltages, distances, and air flow for all electrospinning rounds. For TEM studies, single aligned fiber arrays were wound around a microtomable epoxy substrate and sputter-coated with 15 nm of gold. Single fibers were removed from the double-rod collector using twisted pipe cleaners coated with double-sided tape and subsequently taped and glued directly onto cardboard tabs with diamond-shaped cutouts for mechanical tests.

Tensile Testing and Diameter Measurements on Fibers and Films. Single fibers in an aligned array were removed from the double-rod collector using twisted pipe cleaners coated with double-sided tape, and subsequently taped and glued with epoxy directly onto small cardboard tabs (10 mm × 5 mm) with diamond-cut openings for mechanical tests. Care was taken to minimize damage to fibers during collection. However, variation in fiber structure may arise from varying electric fields along the double-rod collector, as well as from variations in QD dispersion in the polymer.[14] The diameters of the fibers were imaged and photographed using a 63× objective lens on a standard optical microscope (QCapture camera and QImaging software) which was calibrated using a TEM grid (17.97 pixels/μm). The fiber diameters were analyzed using ImageJ. Uniaxial tensile testing was performed using an Agilent T150 nanomechanical tensile tester. The strain rate was set to 6.9×10^{-3} for all runs. The average fiber diameter, measured over 20−25 samples, was approximately ∼4 ± 1 μm for all concentrations. The gauge lengths, measured with digital calipers, were between 6 and 10 mm. No dependence of the Young's modulus on the gauge length or diameter in this range was found. To obtain a statistical average of the values of the Young's modulus, we conducted between 10 and 15 tests per concentration.

Transmission Electron Microscopy (TEM) Imaging and Sample Preparation. Electrospun fiber mats and/or films of polymer nanocomposites were deposited onto microtomable epoxy substrates and then embedded in epoxy stained with rhodamine 6G and cured overnight at 60 °C. An ultramicrotome was used to cut ∼60 nm thin sections, which were floated onto copper TEM grids from water. These sections were then imaged in a FEI Tecnai 12 TEM at an accelerating voltage of 120 kV or a FEI Tecnai G2 TEM at 200 kV.

Simulation Methods. LSMs are an alternative to finite element models[14,63] and have been shown to reproduce the equations of elasticity for an isotropic elastic medium.[62] While we use a 2D model here, studies comparing numerous 2D and 3D lattice spring models have shown that, in the elastic limit, the results from 2D LSMs agreed with those from 3D models to within 5−10%, with considerable saving in computational time.[68]

Using the literature value for the Young's modulus of CdSe (E = 50 GPa),[69] and our experimentally measured Young's modulus of electrospun SEBS (E = 45 MPa), we set the QD spring constants to be ∼1100 times greater than the polymer spring constant (little to no change was seen in setting the QD spring constant 10−4000 times that of the polymer matrix).[14] Because the "like−like" interaction between the QD ligands and the poly(ethylene-butylene) (PEB) domains of the polymer may resemble a QD ligand interdigitation interaction, we used ligand/interfacial spring constants that were half the polymer spring constant (see ref 3 for simulations of other interface strengths). Once QDs were assigned spring constants and placed in the matrix, the LSM calculated the minimum elastic energy of the spring network under a tensile force, reporting the Young's modulus and Poisson's ratio equilibrium spring configuration under stress.[62]

Other assumptions used in the simulation were also mostly derived from experimental observations. They included the following: (i) the simulated aggregate size in 5, 10, and 20 wt % QD nanocomposites was assumed to scale with the average aggregate size from our TEM images of the samples (SI Figure 2); (ii) aggregates in the QD nanocomposite simulations were placed into an interdigitated hexagonally close-packed (HCP) array, as shown previously.[70] These HCP aggregates were arbitrarily chosen to be square-shaped, since TEM images (Figure 2) showed no particular aggregate shape. Changing the aggregate shape and packing morphology (i.e., randomly packing the QDs) did not appreciably affect the simulation results (SI Figure 4), indicating that the packing density does not play a crucial role in the mechanical properties of these composites. We believe this is because the cavities effectively isolate the QDs from most of the polymer matrix.

The nanometer−node equivalency (the number of nodes in the LSM corresponding to nanometers in the nanocomposites) was 0.4 nm/node for both large ∼13 nm and small ∼4 nm QDs, and the matrix sizes varied from 120 × 120 nodes to 120 × 450 nodes. Node−nanometer equivalencies of 0.4−3 nm/node were not found to impact results as long as the fill factor and cavity size and shape were not changed. Furthermore, each particle was surrounded by a one-node wide interface region represented by nodes with a spring constant of 0.5. Simulations for NRs and TPs were all conducted with a constant matrix size of 156 × 156 nodes.[14] The matrix size was similarly not found to affect results, although smaller matrices were used to save computational time. Further details on the LSM simulation methods are described elsewhere.[14]

■ ASSOCIATED CONTENT

Supporting Information

The Supporting Information is available free of charge on the ACS Publications website at DOI: 10.1021/acs.chemmater.5b04165.

Simulations and experiments on additional cavitated nanocomposite systems, stress−strain curves of the QD−SEBS nanocomposites, and additional information (PDF)

■ AUTHOR INFORMATION

Corresponding Authors

*(A.P.A.) E-mail: apalivisatos@lbl.gov.
*(R.O.R.) E-mail: roritchie@lbl.gov.

Funding

This work was supported by the "Self-Assembly of Organic/Inorganic Nanocomposite Materials" program, Office of Science, the Office of Basic Energy Sciences (BES), Materials Sciences and Engineering (MSE) Division of the U.S. Department of Energy (DOE), under Contract No. DE-AC02-05CH11231. The electrospinning work, performed by L.L., was supported by NSF Grant ECCS-0901864.

Notes

The authors declare no competing financial interest.

■ ACKNOWLEDGMENTS

The authors would like to thank Peter Ercius, Ting Xu, and Danny Hellebusch for helpful discussions. They also thank Kari Thorkelsson, Tina Ding, Andrew C. K. Olson, Yinyin Amy Lu, Lillian Hsueh, Turner Anderson, Jackson J. Huang, and Christina M. Hyland for experimental assistance, Aditya Limaye, David Mrdjenovich, Prof. Anna Balazs, and Prof. Gavin Buxton for numerical modeling assistance, and Ziqi Chen for assistance with the figures.

■ REFERENCES

(1) Ishiyama, C.; Higo, Y. Effects of humidity on Young's modulus in poly(methyl methacrylate). *J. Polym. Sci., Part B: Polym. Phys.* **2002**, *40*, 460−465.

(2) Novak, B. M. Hybrid nanocomposite materials—between inorganic glasses and organic polymers. *Adv. Mater.* **1993**, *5*, 422−433.

(3) Sato, Y.; Furukawa, J. Molecular theory of filler reinforcement based upon the conception of internal deformation (a rough

DOI: 10.1021/acs.chemmater.5b04165
Chem. Mater. 2016, 28, 2540−2549

approximation of the internal deformation). *Rubber Chem. Technol.* **1963**, *36*, 1081−1106.
(4) Li, X.; Ono, T.; Wang, Y.; Esashi, M. Ultrathin single-crystalline-silicon cantilever resonators: fabrication technology and significant specimen size effect on Young's modulus. *Appl. Phys. Lett.* **2003**, *83*, 3081.
(5) Ramanathan, T.; Abdala, A. A.; Stankovich, S.; Dikin, D. A.; Herrera-Alonso, M.; Piner, R. D.; Adamson, D. H.; Schniepp, H. C.; Chen, X.; Ruoff, R. S.; Nguyen, S. T.; Aksay, I. A.; Prud'Homme, R. K.; Brinson, L. C. *Nat. Nanotechnol.* **2008**, *3*, 327−331.
(6) Prasad, K. E.; Das, B.; Maitra, U.; Ramamurty, U.; Rao, C. N. R. *Proc. Natl. Acad. Sci. U. S. A.* **2009**, *106*, 13186−13189.
(7) Balazs, A. C.; Emrick, T.; Russell, T. P. Nanoparticle polymer composites: where two small worlds meet. *Science* **2006**, *314*, 1107−1110.
(8) Nielsen, L. Mechanical properties of particulate-filled systems. *J. Compos. Mater.* **1967**, *1*, 100−119.
(9) Raja, S. N.; Olson, A. C. K.; Thorkelsson, K.; Luong, A. J.; Hsueh, L.; Chang, G.; Gludovatz, B.; Lin, L.; Xu, T.; Ritchie, R. O.; Alivisatos, A. P. *Nano Lett.* **2013**, *13*, 3915−3922.
(10) Ciprari, D.; Jacob, K.; Tannenbaum, R. *Macromolecules* **2006**, *39*, 6565−6573.
(11) Kim, J. Y.; Raja, S.; Stellacci, F. Evolution of Langmuir Film of Nanoparticles Through Successive Compression Cycles. *Small* **2011**, *7*, 2526−2532.
(12) Luo, J. Young's modulus of electroplated Ni thin film for MEMS applications. *Mater. Lett.* **2004**, *58*, 2306−2309.
(13) Lan, T.; Pinnavaia, T. J. Clay-reinforced epoxy nanocomposites. *Chem. Mater.* **1994**, *6*, 2216−2219.
(14) Raja, S. N.; Olson, A. C. K.; Limaye, A. M.; Thorkelsson, K.; Luong, A.; Lin, L.; Ritchie, R. O.; Xu, T.; Alivisatos, A. P. Influence of three-dimensional nanoparticle branching on the Young's modulus of nanocomposites: Effect of interface orientation. *Proc. Natl. Acad. Sci. U. S. A.* **2015**, *112*, 6533−6538.
(15) Jin, X.; Deng, M.; Kaps, S.; Zhu, X.; Hölken, I.; Mess, K.; Adelung, R.; Mishra, Y. K. Study of Tetrapodal ZnO-PDMS Composites: A comparison of fillers shapes in stiffness and hydrophobicity improvements. *PLoS One* **2014**, *9*, e106991.
(16) Peng, F.; Shaw, M. T.; Olson, J. R.; Wei, M. Hydroxyapatite Needle-Shaped Particles/Poly(l-lactic acid) Electrospun scaffolds with perfect particle-along-nanofiber orientation and significantly enhanced mechanical properties. *J. Phys. Chem. C* **2011**, *115*, 15743−15751.
(17) Rafiee, M. A.; Rafiee, J.; Wang, Z.; Song, H.; Yu, Z.-Z.; Koratkar, N. *ACS Nano* **2009**, *3*, 3884−3890.
(18) Coleman, J. N.; Khan, U.; Gun'ko, Y. K. Mechanical reinforcement of polymers using carbon nanotubes. *Adv. Mater.* **2006**, *18*, 689.
(19) Sau, K. P.; Chaki, T. K.; Khastgir, D. Electrical and mechanical properties of conducting carbon black filled composites based on rubber and rubber blends. *J. Appl. Polym. Sci.* **1999**, *71*, 887−895.
(20) Heinrich, G.; Vilgis, T. A. Contribution of entanglements to the mechanical properties of carbon black-filled polymer networks. *Macromolecules* **1993**, *26*, 1109−1119.
(21) Laura, D. M.; Keskkula, H.; Barlow, J. W.; Paul, D. R. Effect of glass fiber surface chemistry on the mechanical properties of glass fiber reinforced, rubber-toughened nylon 6. *Polymer* **2002**, *43*, 4673.
(22) Crosby, A. J.; Lee, J. Y. Polymer Nanocomposites: The 'nano' effect on mechanical properties. *Polym. Rev.* **2007**, *47*, 217−229.
(23) Raja, S. N.; Basu, S.; Limaye, A. M.; Anderson, T. J.; Hyland, C. M.; Lin, L.; Alivisatos, A. P.; Ritchie, R. O. Strain-dependent dynamic mechanical properties of Kevlar to failure: Structural correlations and comparisons to other polymers. *Mater. Today Commun.* **2015**, *2*, e33−e37.
(24) Dair, B. J.; Honeker, C. C.; Alward, D. B.; Avgeropoulos, A.; Hadjichristidis, N.; Fetters, L. J.; Capel, M.; Thomas, E. L. Mechanical properties and deformation behavior of the double gyroid phase in unoriented thermoplastic elastomers. *Macromolecules* **1999**, *32*, 8145−8152.
(25) Tjong, S. C. Structural and mechanical properties of polymer nanocomposites. *Mater. Sci. Eng., R* **2006**, *53*, 73.
(26) Coleman, J. N.; Khan, U.; Blau, W. J.; Gun'ko, Y. K. *Carbon* **2006**, *44*, 1624−1652.
(27) Kojima, Y.; Usuki, A.; Kawasumi, M.; Okada, A.; Fukushima, Y.; Kurauchi, T.; Kamigaito, O. *J. Mater. Res.* **1993**, *8*, 1185−1189.
(28) Callister, W. D.; Rethwisch, D. G. *Fundamentals of Materials Science and Engineering*; John Wiley & Sons: 2012.
(29) Choi, J.; Shin, H.; Yang, S.; Cho, M. The influence of nanoparticle size on the mechanical properties of polymer nanocomposites and the associated interphase region: A multiscale approach. *Compos. Struct.* **2015**, *119*, 365−376.
(30) Laura, D. M.; Keskkula, H.; Barlow, J. W.; Paul, D. R. Effect of rubber particle size and rubber type on the mechanical properties of glass fiber reinforced, rubber-toughened nylon 6. *Polymer* **2003**, *44*, 3347−3361.
(31) B cu-Longuet, L.; Bonnet, A.; Pichot, C.; Sautereau, H.; Maazouz, A. Epoxy networks toughened by core-shell particles: Influence of the particle structure and size on the rheological and mechanical properties. *J. Appl. Polym. Sci.* **1999**, *72*, 849−858.
(32) Pawlak, A.; Galeski, A. Cavitation during tensile deformation of polypropylene. *Macromolecules* **2008**, *41*, 2839−2851.
(33) Pawlak, A. Cavitation during deformation of polymers on the example of polypropylene. *J. Appl. Polym. Sci.* **2012**, *125*, 4177−4187.
(34) Pawlak, A.; Rozanski, A.; Galeski, A. Thermovision studies of plastic deformation and cavitation in polypropylene. *Mech. Mater.* **2013**, *67*, 104−118.
(35) Makke, A.; Perez, M.; Rottler, J.; Lame, O.; Barrat, J.-L. Predictors of cavitation in glassy polymers under tensile strain: A coarse-grained molecular dynamics investigation. *Macromol. Theory Simul.* **2011**, *20*, 826−836.
(36) Capadona, J. R.; Shanmuganathan, K.; Tyler, D. J.; Rowan, S. J.; Weder, C. Stimuli-responsive polymer nanocomposites inspired by the sea cucumber dermis. *Science* **2008**, *319*, 1370−1374.
(37) Toepperwein, G. N.; de Pablo, J. J. Cavitation and crazing in rod-containing nanocomposites. *Macromolecules* **2011**, *44*, 5498−5509.
(38) Neitzel, I.; Mochalin, V. N.; Niu, J.; Cuadra, J.; Kontsos, A.; Palmese, G. R.; Gogotsi, Y. Maximizing Young's modulus of aminated nanodiamond-epoxy composites measured in compression. *Polymer* **2012**, *53*, 5965−5971.
(39) Wutticharoenmongkol, P.; Sanchavanakit, N.; Pavasant, P.; Supaphol, P. Novel bone scaffolds of electrospun polycaprolactone fibers filled with nanoparticles. *J. Nanosci. Nanotechnol.* **2006**, *6*, 514−522.
(40) Yang, L.; Fitié, C. F. C.; van der Werf, K. O.; Bennink, M. L.; Dijkstra, P. J.; Feijen, J. Mechanical properties of single electrospun collagen type I fibers. *Biomaterials* **2008**, *29*, 955−962.
(41) Behler, K. D.; Stravato, A.; Mochalin, V.; Korneva, G.; Yushin, G.; Gogotsi, Y. Nanodiamond-polymer composite fibers and coatings. *ACS Nano* **2009**, *3*, 363−369.
(42) Greiner, A.; Wendorff, J. H. Electrospinning: A fascinating method for the preparation of ultrathin fibers. *Angew. Chem., Int. Ed.* **2007**, *46*, 5670−5703.
(43) Ramakrishna, S. *An Introduction to Electrospinning and Nanofibers*; World Scientific: 2005.
(44) Zhu, L.; Liang, K.; Ji, Y. Prominent reinforcing effect of chitin nanocrystals on electrospun polydioxanone nanocomposite fiber mats. *J. Mech. Behav. Biomed. Mater.* **2015**, *44*, 35−42.
(45) Camposeo, A.; Greenfeld, I.; Tantussi, F.; Pagliara, S.; Moffa, M.; Fuso, F.; Allegrini, M.; Zussman, E.; Pisignano, D. Local mechanical properties of electrospun fibers correlate to their internal nanostructure. *Nano Lett.* **2013**, *13*, 5056−5062.
(46) Talapin, D. V.; Nelson, J. H.; Shevchenko, E. V.; Aloni, S.; Sadtler, B.; Alivisatos, A. P. Seeded growth of highly luminescent CdSe/CdS nanoheterostructures with rod and tetrapod morphologies. *Nano Lett.* **2007**, *7*, 2951−2959.
(47) Chen, O.; Zhao, J.; Chauhan, V. P.; Cui, J.; Wong, C.; Harris, D. K.; Wei, H.; Han, H.-S.; Fukumura, D.; Jain, R. K.; Bawendi, M. G. Compact high-quality CdSe−CdS core−shell nanocrystals with

DOI: 10.1021/acs.chemmater.5b04165
Chem. Mater. 2016, 28, 2540−2549

narrow emission linewidths and suppressed blinking. *Nat. Mater.* **2013**, *12*, 445−451.
(48) Li, D.; Wang, Y.; Xia, Y. Electrospinning of polymeric and ceramic nanofibers as uniaxially aligned arrays. *Nano Lett.* **2003**, *3*, 1167−1171.
(49) Lewis, T. B.; Nielsen, L. E. Dynamic mechanical properties of particulate-filled composites. *J. Appl. Polym. Sci.* **1970**, *14*, 1449−1471.
(50) Koltisko, B.; Hiltner, A.; Baer, E.; Tung, L. H. Crazing in thin films of styrene−butadiene−styrene block copolymers. *J. Polym. Sci., Part B: Polym. Phys.* **1986**, *24*, 2167−2183.
(51) Agrawal, S.; Patidar, D.; Saxena, N. S. Investigation of temperature-dependent mechanical properties of CdS/PMMA nanocomposites. *J. Compos. Mater.* **2011**, *45*, 2507−2514.
(52) Mathur, V.; Dixit, M.; Rathore, K. S.; Saxena, N. S.; Sharma, K. B. Morphological and mechanical characterization of a PMMA/CdS nanocomposite. *Front. Chem. Sci. Eng.* **2011**, *5*, 258−263.
(53) McCumiskey, E. J.; Chandrasekhar, N.; Taylor, C. R. Nanomechanics of CdSe quantum dot−polymer nanocomposite films. *Nanotechnology* **2010**, *21*, 225703.
(54) Kausch, H. H.; Michler, G. H. Effect of nanoparticle size and size-distribution on mechanical behavior of filled amorphous thermoplastic polymers. *J. Appl. Polym. Sci.* **2007**, *105*, 2577−2587.
(55) Dompas, D.; Groeninckx, G. Toughening behaviour of rubber-modified thermoplastic polymers involving very small rubber particles: 1. A criterion for internal rubber cavitation. *Polymer* **1994**, *35*, 4743.
(56) Bockstaller, M.; Mickiewicz, R.; Thomas, E. Block copolymer nanocomposites: perspectives for tailored functional materials. *Adv. Mater.* **2005**, *17*, 1331−1349.
(57) Seguela, R.; Prud'Homme, J. Deformation mechanism of thermoplastic two-phase elastomers of lamellar morphology having a high volume fraction of rubbery microphase. *Macromolecules* **1981**, *14*, 197−202.
(58) Chen, J.-K.; Wang, G.-T.; Yu, Z.-Z.; Huang, Z.; Mai, Y.-W. Critical particle size for interfacial debonding in polymer/nanoparticle composites. *Compos. Sci. Technol.* **2010**, *70*, 861−872.
(59) Nielsen, L. E. Cross-linking−effect on physical properties of polymers. *J. Macromol. Sci., Polym. Rev.* **1969**, *3*, 69−103.
(60) Dorfmann, A.; Fuller, K. N. G.; Ogden, R. W. Shear, compressive and dilatational response of rubberlike solids subject to cavitation damage. *Int. J. Solids Struct.* **2002**, *39*, 1845−1861.
(61) Wendorff, J. H.; Agarwal, S.; Greiner, A. *Electrospinning*; John Wiley & Sons: 2012.
(62) Buxton, G. A.; Care, C. M.; Cleaver, D. J. *Modell. Simul. Mater. Sci. Eng.* **2001**, *9*, 485−497.
(63) Ostoja-Starzewski, M. Lattice models in micromechanics. *Appl. Mech. Rev.* **2002**, *55*, 35−60.
(64) Buxton, G. A.; Balazs, A. C. Predicting the mechanical properties of binary blends of immiscible polymers. *Interface Sci.* **2003**, *11*, 175−186.
(65) Buxton, G.; Balazs, A. Modeling the dynamic fracture of polymer blends processed under shear. *Phys. Rev. B: Condens. Matter Mater. Phys.* **2004**, *69*, 054101.
(66) Buxton, G. A.; Balazs, A. C. Predicting the mechanical and electrical properties of nanocomposites formed from polymer blends and nanorods. *Mol. Simul.* **2004**, *30*, 249−257.
(67) Buxton, G.; Balazs, A. Simulating the morphology and mechanical properties of filled diblock copolymers. *Phys. Rev. E: Stat. Phys., Plasmas, Fluids, Relat. Interdiscip. Top.* **2003**, *67*, 031802.
(68) Böhm, H. J.; Han, W. Comparisons between three-dimensional and two-dimensional multi-particle unit cell models for particle reinforced metal matrix composites. *Modell. Simul. Mater. Sci. Eng.* **2001**, *9*, 47−65.
(69) Kim, F.; Kwan, S.; Akana, J.; Yang, P. Langmuir-Blodgett nanorod assembly. *J. Am. Chem. Soc.* **2001**, *123*, 4360−4361.
(70) Tam, E.; Podsiadlo, P.; Shevchenko, E.; Ogletree, D. F.; Delplancke-Ogletree, M.-P.; Ashby, P. D. Mechanical properties of face-centered cubic supercrystals of nanocrystals. *Nano Lett.* **2010**, *10*, 2363−2367.

DOI: 10.1021/acs.chemmater.5b04165
Chem. Mater. 2016, 28, 2540−2549